Published in final edited form as:

Plant J. 2019 February ; 97(4): 646–660. doi:10.1111/tpj.14148.

The Arabidopsis RRM domain protein EDM3 mediates race-specific disease resistance by controlling H3K9me2-dependent alternative polyadenylation of *RPP7* immune receptor transcripts

Yan Lai[1,2], **Alayne Cuzick**[3,4], **Xueqing M. Lu**[5], **Jianqiang Wang**[1], **Neerja Katiyar**[6], **Tokuji Tsuchiya**[7], **Karine Le Roch**[5], **John M. McDowell**[8], **Eric Holub**[3], **Thomas Eulgem**[1,*]

[1]Department of Botany and Plant Sciences, Center for Plant Cell Biology, Institute of Integrative Genome Biology, University of California at Riverside, Riverside, CA 92521, USA

[2]College of Life Sciences, Fujian Agricultural and Forestry University, Fuzhou, Fujian 350002, China

[3]School of Life Sciences, University of Warwick, Wellesbourne Campus, Warwick CV35 9EF, UK

[4]Biointeractions and Crop Protection, Rothamsted Research, Harpenden AL5 2JQ, UK

[5]Department of Molecular, Cell and Systems Biology, Center for Infectious Disease and Vector Research, Institute of Integrative Genome Biology, University of California at Riverside, Riverside, CA 92521, USA

[6]Institute of Integrative Genome Biology, University of California at Riverside, Riverside, CA 92521, USA

[7]College of Bioresource Sciences, Nihon University, Kanagawa 252-0880, Japan

[8]Department of Plant Pathology, Physiology, and Weed Science, Virginia Tech, Blacksburg, VA 24060-0329, USA

SUMMARY

The NLR-receptor RPP7 mediates race-specific immunity in Arabidopsis. Previous screens for *enhanced downy mildew* (*edm*) mutants identified the co-chaperone SGT1b (EDM1) and the PHD-finger protein EDM2 as critical regulators of RPP7. Here, we describe a third *edm* mutant compromised in *RPP7* immunity, *edm3*. *EDM3* encodes a nuclear-localized protein featuring an RNA-recognition motif. Like EDM2, EDM3 promotes histone H3 lysine 9 dimethylation (H3K9me2) at *RPP7*. Global profiling of H3K9me2 showed EDM3 to affect this silencing mark at a large set of loci. Importantly, both EDM3 and EDM2 co-associate *in vivo* with H3K9me2-marked chromatin and transcripts at a critical proximal polyadenylation site of *RPP7*, where they suppress proximal transcript polyadeylation/termination. Our results highlight the complexity of

*For correspondence (thomas.eulgem@ucr.edu).

CONFLICT OF INTERESTS

The authors declare no competing interests.

SUPPORTING INFORMATION

Additional Supporting Information may be found in the online version of this article.

plant NLR gene regulation, and establish a functional and physical link between a histone mark and NLR-transcript processing.

Keywords

RNA-binding protein; disease-resistance genes; histone-binding proteins; transcript processing; *Hyaloperonospora arabidopsidis*

INTRODUCTION

Disease-resistance (*R*) genes that encode immune receptor proteins are critical for plant immunity against pathogenic microorganisms. *R* genes were originally defined based on their ability to induce race-specific disease resistance leading to incompatible host/pathogen interactions. Functional *R* alleles are typically genetically dominant and encode receptors that mediate recognition of pathogen proteins encoded by genetically dominant avirulence (AVR) alleles (Flor, 1971). Most *R* genes encode NLR proteins with a nucleotide-binding site (NB) and C-terminal leucine-rich repeats (LRR; Jacob *et al.*, 2013; Jones *et al.*, 2016). In *Arabidopsis thaliana* (Arabidopsis), many of these NLR proteins contain either a coiled coil (CC) or a Toll interleukin-1 receptor domain (Meyers *et al.*, 2003) at their N-terminus.

Pathogen *AVR* genes are fast-evolving and encode polymorphic effector proteins that are secreted to the apoplast or the interior of plant cells. Their virulence functions are to interact with host proteins to attenuate host immune responses or otherwise enhance pathogen fitness in the host environment (Abramovitch *et al.*, 2006; Chisholm *et al.*, 2006; Dangl and McDowell, 2006). However, secreted effectors can be recognized by specific NLR immune receptors through direct receptor/ligand interactions or indirect detection of the effector's virulence function (Dangl and McDowell, 2006). Such recognition elicits a powerful set of immune responses collectively referred to as effector-triggered immunity (ETI), which often culminates in programmed death of plant cells at the infection site (termed the hypersensitive response or HR). ETI typically protects plants against disease resulting in incompatibility between host and pathogen.

Proper homeostasis of NLR activity is critical for the function of these immune receptors (Li *et al.*, 2015). Gene dosage experiments have demonstrated that NLR protein levels must be above a certain threshold to robustly activate defense signaling (Bieri *et al.*, 2004; Holt *et al.*, 2005). On the other hand, mutations that either constitutively activate NLR proteins or result in elevated NLR transcript or protein levels can lead to embryo lethality, spontaneous cell death and/or stunted plant growth, due to ectopic activation of immune responses (Shirano *et al.*, 2002; Mackey *et al.*, 2003; Xiao *et al.*, 2003; Palma *et al.*, 2010). In some cases, reduction in plant fitness has been associated with naturally occurring *R* gene alleles (Tian *et al.*, 2003; Korves and Bergelson, 2004; Karasov *et al.*, 2014). Finally, the phenomenon of hybrid necrosis can be caused by aberrant genetic interactions involving NLR genes in hybrid genomes. Imbalanced activity of NLRs in such hybrid contexts can result in autoimmunity-related phenomena, such as spontaneous HR (Bomblies and Weigel, 2007; Bomblies *et al.*, 2007). Similar effects are often observed in transgenic plant lines overexpressing certain NLRs (Stokes *et al.*, 2002; Li *et al.*, 2015).

These phenomena illustrate that the activity and expression of R proteins must be strictly controlled, to ensure efficient immunity without spurious fitness costs. Accordingly, *R* genes, and their encoded proteins, are tightly regulated at multiple levels. Post-translational mechanisms are known to control NLR protein levels and activity (Hubert *et al.*, 2003; Bieri *et al.*, 2004; Schulze-Lefert, 2004; Holt *et al.*, 2005; Cheng *et al.*, 2011). Besides this, control of NLR transcript levels is important for their function (Mohr *et al.*, 2010). For example, transcript levels of *RPP7* strictly correlate with levels of immunity conferred by this Arabidopsis NLR gene (Tsuchiya and Eulgem, 2011, 2013b). Such dose-dependency is further supported by the incomplete dominance exhibited by some NLR genes, which are unable to confer full levels of immunity, when present only in one copy (Reignault *et al.*, 1996; McDowell *et al.*, 1998; van der Biezen *et al.*, 2002; Holt *et al.*, 2005). Complex interplay of several control mechanisms affecting transcription, co/post-transcriptional processing, and transcript turnover can balance base levels of NLR transcripts and allow for dynamic adjustments in certain biological situations (Lai and Eulgem, 2017).

Race-specific interactions between different accessions of Arabidopsis and distinct isolates of the pathogenic oomycete *Hyaloperonospora arabidopsidis* (causal agent of Arabidopsis downy mildew; formerly *Peronospora parasitica*) have served as a successful model system to study *R* gene-mediated immunity (Holub, 2001, 2008; Anderson *et al.*, 2015). Several race-specific, incompatible interactions for this pathosystem have been established and are widely used (Holub *et al.*, 1994; Tör *et al.*, 1994; Holub, 2008). In some cases, the Arabidopsis *R* genes and *H. arabidopsidis AVR* genes governing the outcome of the respective plant/pathogen interactions have been cloned (Bittner-Eddy *et al.*, 1999; Allen *et al.*, 2004).

The CC-NB-LRR gene *RPP7* of the Arabidopsis accession Columbia (Col) is known to mediate particularly strong disease resistance against the Hiks1 isolate of *H. arabidopsidis* (referred to hence as *Hpa*-Hiks1; McDowell *et al.*, 2000; Eulgem *et al.*, 2007). In order to identify Arabidopsis genes required for *RPP7*-mediated immunity, screens have been performed using *Hpa*-Hiks1 for *enhanced downy mildew* (*edm*) susceptibility mutants in Col. Besides numerous mutant *rpp7* alleles, mutations were identified in genes encoding the general NLR co-chaperone SGT1b (EDM1) and the histone-binding PHD-finger protein EDM2 (Tör *et al.*, 2002; Eulgem *et al.*, 2007).

A large body of literature now supports roles of Arabidopsis SGT1b and some of its orthologs in other species as co-chaperones controlling protein stability of several NLRs. While details of its involvement in RPP7 regulation are unknown, SGT1b acts as a positive regulator of *RPP7*-mediated immunity (Tör *et al.*, 2002).

EDM2 is a nuclear protein featuring 2½ repeats of an atypical PHD-finger motif, several acidic domains, a motif related to replication foci domains, a plant G gamma-like-related domain, an N6-adenine methyltransferase-like domain conserved in EDM2-like plant proteins (ELP domain), and a proline-rich C-terminal region (Eulgem *et al.*, 2007; Tsuchiya and Eulgem, 2010a; Lei *et al.*, 2013). EDM2 positively controls levels of RPP7 protein-coding transcripts, which correlate with levels of immunity mediated by this NLR gene (Eulgem *et al.*, 2007; Tsuchiya and Eulgem, 2011, 2013b). *In vitro* the 2½ PHD-finger

module of EDM2 can bind to histone H3 proteins that are simultaneously marked by post-translational acetylation or mono-, di- or tri-methylation at lysine residues 4 and 9 (K4 and K9; Tsuchiya and Eulgem, 2014). We further found that EDM2 modulates histone H3 lysine 9 dimethylation (H3K9me2) levels to control silencing of transposable elements (TEs; Tsuchiya and Eulgem, 2013a,b). Besides being compromised in *RPP7*-mediated immunity, mutants of EDM2 exhibit several developmental phenotypes (Tsuchiya and Eulgem, 2010b). Trans-generational variability and instability of such phenotypes (Tsuchiya and Eulgem, 2013a) suggested roles of EDM2 in epigenetic processes.

EDM2 affects levels of *RPP7* protein-coding transcripts by controlling alternative polyadenylation (Tsuchiya and Eulgem, 2013b). EDM2 promotes high levels of H3K9me2 at a transposon-associated proximal polyadenylation site in the first *RPP7* intron and suppresses its use, thereby repressing a non-coding transcript and promoting high levels of RPP7 transcripts that encode the full-length NLR protein. We further showed that this EDM2- and H3K9me2-dependent alternative polyadenylation mechanism is activated by *H. arabidopsidis* recognition and dynamically adjusts *RPP7* expression levels during the induction of immune responses. Genome-wide profiling of *edm2* mutants by bisulfite-seq showed EDM2 to globally suppress levels of methylated cytosine in genic regions bordering heterochromatic repeats or transposons (Lei *et al.*, 2013).

Here, we report the map-based cloning of a third *Hpa*-Hiks1 susceptibility mutation in the *EDM3* gene. We show that *EDM3* encodes a protein with an RNA recognition motif (RRM). During the final stages of completion of this manuscript, Duan *et al.* (2017) reported on the identification of the RRM domain protein AIPP1, which is identical to EDM3, as a likely *in vivo* interactor of EDM2. Physical interactions between AIPP1 and EDM2 were demonstrated by various assays, and genome-wide effects of both regulators on cytosine-methylation were shown to be similar. However, the absence of a clear biological phenotype of *aipp1* mutants in the report by Duan *et al.* (2017) leaves the biological significance of AIPP1 and its interactions with EDM2 unclear. We provide genetic evidence that the *EDM3/AIPP1* gene is a critical contributor to race-specific immunity of Arabidopsis against *Hpa*-Hiks1. We show that, like *EDM2*, *EDM3* controls alternative polyadenylation of *RPP7* immune receptor transcripts by suppressing proximal polyadenylation at a transposon insertion site in the first *RPP7* intron. Furthermore, we found EDM3 and EDM2 to co-associate *in vivo* with RPP7 transcripts and chromatin at a critical proximal polyadenylation site.

RESULTS

Identification and characterization of the *edm3–1* mutant

The *edm3–1* mutant was identified in a screen of approximately 50 000 M2 mutant seedlings, derived from 6000 M1 Col-5 (*glabrous-1* mutant of the parental Col-0 accession) plants subjected to fast-neutron bombardment (Lehle seeds), for *Hpa*-Hiks1-susceptible individuals. We compared levels of *Hpa*-Hiks1 susceptibility of *edm3–1* with its resistant parent (Col-5), two wild-type *Hpa*-Hiks1 susceptible ecotypes (Duc-1, Ksk-1), and the previously characterized *rpp7–1* and *edm2–1* mutants (McDowell *et al.*, 2000; Eulgem *et al.*, 2007). The enhanced disease susceptibility mutant in the Ws-0 ecotype (Ws-*eds1*) was also

included for comparison as a control known to be strongly susceptible against various different *H. arabidopsidis* isolates (Parker *et al.*, 1996). Like *rpp7–1* and *edm2–1*, *edm3–1* plants supported sporulation of *Hpa*-Hiks1 at levels similar to the two susceptible wild-type accessions and Ws-*eds1*, while Col-5 plants exhibited tight resistance not allowing for detectable levels of *Hpa*-Hiks1 sporulation (Table 1). Mutant phenotypes of representative cotyledons are shown in Figure 1.

We further tested the mutants for susceptibility to *the H. arabidopsidis* isolates Cala2 and Cand5, each recognized by different *RPP* specificities in Columbia (Sinapidou *et al.*, 2004). All three tested Col-5 mutants (*rpp7–1*, *edm2–1* and *edm3–1*) were unaffected in resistance to *Hpa*-Cala2 and *Hpa*-Cand5, like Col-5 allowing on average for the development of less than one sporangiophore per cotyledon, while Ws-*eds1* plants exhibited full susceptibility against both *H. arabidopsidis* isolates (Table 1). Thus, like *rpp7–1 and edm2–1, edm3–1* plants are clearly compromised in a mechanism conferring race-specific disease resistance of the Col accession against *Hpa*-Hiks1.

A prominent molecular phenotype associated with loss of *RPP7* immunity in *edm2* mutants is a low ratio between levels of *RPP7* full-length coding transcripts and the proximal-polyadenylated, non-coding ECL (exon 1-containing LTR-terminated) transcript produced at the *RPP7* locus (Tsuchiya and Eulgem, 2013b). We observed in *edm3–1* an equally low ratio between these two *RPP7* transcript isoforms (Figure 2a). Consequently, in both mutants, the levels of *RPP7* coding transcripts are substantially lower than in Col-5 (Figure S1).

We backcrossed *edm3–1* plants to glabrate (trichome-bearing) Col-0 (*GL1*/*RPP7*) plants. F_1 hybrids from crosses involving the mutant as the female and Col-0 as the male were glabrate, indicating a successful out-cross rather than contaminant pollination. Reciprocal crosses for all mutants were also tested at the F_1 generation. No differences were observed between reciprocal back-crosses for each mutant, with a mean sporulation of < 1 sporangiophore/cotyledon in each case (Table S1). This level of sporulation, compared with the strict absence of sporulation in Col-5, indicates that the *edm3–1* mutation is recessive, but that heterozygotes are slightly less effective in resistance to *Hpa*-Hiks1 than in wild-type Col-5. Thus, the wild-type allele is incompletely dominant. The analysis of segregation in the F_2 generation yielded an observed ratio of three resistant to one susceptible plants, confirming that the *edm3–1* mutant phenotype is caused by a single, recessive allele ($P > 0.05$ for expected 3:1 ratio; Table S1). Similarities of the molecular, microscopic and macroscopic defense-related phenotypes of the e*dm2* and *edm3* mutants (Figures 1, 2a and S1; Table 1) suggested that both genes affect related steps in the regulation of *RPP7* expression. The strong *Hpa*-Hiks1 susceptibility phenotype of *edm3* demonstrates that this gene is essential for *RPP7* resistance.

Map-based cloning of *EDM3*

To determine the map position of the *edm3* mutation, we generated an F_2 population from a cross of *edm3–1* (in Col-5 background) to wild-type plants of the Landsberg *erecta* (Ler) accession. Ler contains a functional allele of *RPP7* (Tör *et al.*, 2002), thus *edm3* was the only locus segregating for *Hpa*-Hiks1 susceptibility in this cross. Using 278 *Hpa*-Hiks1 susceptible F_2s from this cross, we mapped *EDM3* to an approximately 8 Mbp interval on

the top arm of chromosome 1, between the molecular markers nga59 and ciw12 (Lukowitz *et al.*, 2000). Sequencing the genomes of *edm3–1* and Col-5 by Illumina MiSeq followed by variant analysis uncovered only one mutation in *edm3–1* affecting predicted coding sequences in the nga59-ciw12 interval: an in-frame deletion of two codons (6 bp) in the first of two coding exons of At1g05970 (Figures 2b and c, and S2). In TAIR10, At1g05970 is annotated as expressing two transcript isoforms (At1g05970–1 and At1g05970–2) encoding proteins of predicted molecular weights of 22.65 and 22.91 kDa, respectively. Relative to isoform 1, isoform 2 contains two additional codons (six additional coding nucleotides) at the 5' end of exon 2 (Figure S2). Thus, both proteins predicted to be encoded by this gene have identical N- and C-terminal portions, and differ only in the presence/absence of two amino acids in the central region (Figure 2c). The *edm3–1* mutation affects both isoforms.

To confirm that the mutation in At1g05970 causes the *edm3* phenotype, we transformed *edm3–1* with T-DNA constructs (Figure 2d) harboring genomic fragments containing the entire At1g05970 transcribed region, including intergenic sequences comprising 834 bp upstream from its predicted transcription start site (construct *pE3l::E3g*) or 117 bp upstream from this site (until next upstream gene At1g05980; construct *pE3s::E3g*). Wild-type levels of resistance to *Hpa*-Hiks1 and RPP7-coding transcripts were restored to *edm3–1* by both constructs (Figure S1). These two constructs also restored the wild-type ratio between *RPP7* full-length coding transcripts and the proximal-polyadenylated, non-coding ECL transcript (Figure 2a). The extent of this effect correlated well with levels of *EDM3* transgene expression in the respective complementation lines (Figure S3). Transgenic rescue of these two *edm3* phenotypes demonstrates that At1g05970 is the *EDM3* gene. At1g05970 is distinct from the *RPP7*, *SGT1b* and *EDM2* loci (At1g58602, At4g11260 and At5g55390, respectively). No mutants with insertions in *EDM3* are publically available.

Both EDM3 protein isoforms are localized to nuclei

In order to determine the subcellular localization of EDM3 proteins, we stably expressed cDNA constructs of its two isoforms as N-terminal green fluorescent protein (GFP) fusions (*p2x35S::GFP-E3cds-1* and *p2x35S::GFP-E3cds-2*; Figure 2d) in the *edm3–1* mutant. Lines expressing either of the two isoforms exhibited near wild-type levels of RPP7-coding transcripts and resistance to *Hpa*-Hiks1, indicating that each isoform can complement the *edm3–1* mutation and is able to execute functions of wild-type EDM3 (Figure S1). Using one line for each isoform (*p2x35S::GFP-E3cds-1–1* and *p2x35S::GFP-E3cds-2–1*), we found both types of EDM3-GFP fusion proteins to be clearly localized to nuclei (Figure 3). We did not observe detectable levels of cytoplasmic localization of either one of the tested GFP-EDM3 fusions, while the control line expressing only GFP exhibited green fluorescence in both nuclear and cytoplasmic regions. The successful functional complementation observed with both EDM3-GFP fusions indicated that the nucleus is the authentic site of EDM3 localization and function.

Based on the predicted molecular weight of approximately 49 kDa for both tested GFP-EDM3 fusion proteins, which is below the 60 kDa free diffusion limit of nuclear pores (Wang and Brattain, 2007), and the lack of obvious nuclear localization signals in both EDM3 isoforms, we had expected the GFP-fusions to be cytoplasmic and nuclear. Either

cryptic nuclear localization signals or tight associations with actively nuclear-targeted proteins may be responsible for the strict nuclear localization we observed for both EDM3-GFP fusions.

The observation that both EDM3 isoforms as GFP fusions can functionally complement the *edm3–1* mutation is consistent with results we observed with other EDM3 isoform-specific expression construct (e.g. *p35S::FLAG-E3cds1* or *p35S::FLAG-E3cds2*; Figure 2d), which also restored wild-type levels of *RPP7* function and expression in the *edm3–1* mutant background (Figure S1). Thus, each of the two EDM3 isoforms seems to be sufficient for proper *RPP7* regulation.

EDM3 promotes H3K9me2 at the proximal *RPP7* polyadenylation site

Our previous work demonstrated that EDM2 regulates *RPP7* expression and function by suppressing proximal transcript polyadenylation/termination at the 5'LTR (long terminal repeat) of the *COPIA-R7* retrotransposon in the 1st *RPP7* intron (Tsuchiya and Eulgem, 2013b). Alternative polyadenylation at this site gives rise to the non-coding ECL transcript and consequently reduces levels of full-length *RPP7* coding transcripts. *COPIA-R7* has recruited the epigenetic transposon silencing mark H3K9me2 into the context of this area at *RPP7*, where it suppresses use of the proximal polyadenylation site. We tested by chromatin immunoprecipitation (ChIP) combined with quantitative real-time polymerase chain reaction (qRT-PCR) whether or not the levels of H3K9me2 are reduced in *edm3–1* at the *COPIA-R7* 5'LTR (Figure 4a and b), and found this to be the case, similar to *edm2* mutants. The transgenic *pE3S::E3g-FLAG-1* line (Figure 2d), which encodes both EDM3 isoforms fused to FLAG (here collectively referred to as EDM3-FLAG) in the *edm3–1* background, restored wild-type H3K9me2 levels in this area (Figure 4b). This line also complemented defense-associated phenotypes of *edm3–1* (Figure S1). Reduced H3K9me2 levels in *edm3–1* at *RPP7* intron 1/COPIA-R7 are consistent with the effect of *EDM3* on the ratio between *RPP7* full-length coding transcript and ECL transcripts (Figure 2a), which we showed previously to be H3K9me2-dependent. These observations further confirm close functional interactions between EDM2 and EDM3.

EDM3 and EDM2 co-associate *in vivo* with *RPP7* chromatin at the proximal polyadenylation site

We previously showed by ChIP-qRT-PCR that EDM2 associates *in vivo* with *RPP7* chromatin surrounding *COPIA-R7* (Tsuchiya and Eulgem, 2013b). We also observed, by ChIP-qRT-PCR with *pE3s::E3g-FLAG-1* plants, a clear *in vivo* association of EDM3-FLAG with the *COPIA-R7* region of *RPP7* (Figure 4c). The highest levels of enrichment with immunoprecipitated chromatin were observed for region 5, which is immediately upstream of the proximal polyadenylation site at the *COPIA-R7* 5'LTR.

EDM3 and EDM2 also co-associate *in vivo* with *RPP7* transcripts at the proximal polyadenylation site

Both of the EDM3 isoforms contain an RRM (Figure 2c). To test if in *pE3s::E3g-FLAG-1* plants EDM3-FLAG can associate *in vivo* with *RPP7* mRNA, we performed RNA immunoprecipitation (RIP) coupled with qRT-PCR. We observed a clear association of

EDM3-FLAG with transcript fragments containing the *COPIA-R7* 5'LTR region (Figure 4d, regions 4–6), but not *RPP7* regions upstream or downstream from this. We also did not observe any association of EDM3-FLAG with transcripts at the distal *RPP7* polyadenylation site in the 9th exon of this gene. Thus, EDM3-FLAG specifically associates with *RPP7* transcripts at the proximal *RPP7* polyadenylation site. We further performed RIP-qRT-PCR with HA-EDM2 using our *edm2–2/E2pro:HA-E2c* complementation line (Tsuchiya and Eulgem, 2013b). Interestingly, we found HA-EDM2 to exhibit a pronounced association with transcripts covering the same area that associates with EDM3-FLAG (Figure 4e). As in the case of EDM3-FLAG, we did not observe any association of HA-EDM2 with the distal *RPP7* polyadenylation site area. Taken together, our data demonstrate that EDM2 and EDM3 co-associate, *in vivo,* with *RPP7* transcripts containing the ECL exon2 area that includes the proximal polyadenylation site. The corresponding genomic area is also marked by EDM2- and EDM3-dependent H3K9me2. The fact that EDM3 and EDM2 co-associate *in vivo* with *RPP7* chromatin and transcripts is consistent with the direct interactions between both proteins demonstrated by Duan *et al.* (2017).

Genome-wide effects of *EDM3* on H3K9me2

Profiling genome-wide effects of *EDM3* on H3K9me2 by ChIP-seq with *edm3–1* plants and their parental Col-5 background, we found a number of loci affected (303 genes and 66 transposons; Tables S2 and S3). Surprisingly, the *edm3–1* mutant displayed hyper-dimethylation in the vast majority of affected genes (299 genes hyper-H3K9 dimethylated, four genes hypo-H3K9 dimethylated). Thus, *EDM3* frequently has a suppressive role in controlling this mark in the context of genes. This is in contrast to the situation at *RPP7*, where EDM3 promotes high levels of H3K9me2. Gene ontology (GO) analysis showed that genes exhibiting H3K9 hyper-dimethylation in *edm3–1* are particularly tightly associated with reproduction, cell cycle, DNA metabolism as well as organization of chromosomes, organelles and cellular components (Figure 5a). Figure 5(b) shows H3K9me2 and transcript patterns at *RPP7/COPIA-R7*. In addition to our ChIP-seq data, we included published RNA-seq results from the *EDM3*-deficient *aipp1–1* line (Duan *et al.*, 2017) for this figure. Relative to its wild-type background (Col-5), *edm3–1* plants exhibit a clear reduction in H3K9me2 levels in the *RPP7* intron 1 area templating for ECL exon 2 as well as the 5' portion of *COPIA-R7*. Deficiency of EDM3 in *aipp1* results in a substantial transcript accumulation in the ECL-templating area and strongly reduced levels of transcripts downstream from the proximal polyadenylation site. These observations are fully consistent with our data shown in Figures 2(a), 4(b) and S1a, showing EDM3 to promote high H3K9me2 levels at the proximal RPP7 polyadenylation site and suppressing use of this transcript termination site. Besides *RPP7*, transcript and/or H3K9me2 levels of 62 additional NLR genes are affected in *edm3* mutants (Table S4).

Taken together, our results show that effects of both *EDM2* and *EDM3* are nearly identical at *RPP7*. Besides affecting *RPP7*, EDM3 has global roles in suppressing H3K9me2.

Enhanced proximal polyadenylation/termination activity at *RPP7* is correlated with increased 2-phospho-serine RNAPII occupancy

We further determined occupancy levels of the actively elongating form of RNA polymerase II (RNAPII), which is phosphorylated at the ser-2 position of the C-terminal domain (CTD) of its largest subunit Rpb1. Performing ChIP with an antibody specifically recognizing 2-phospho-serine CTD/Rpb1, we found occupancy levels of this form of RNAPII to be clearly increased (compared with their respective wild-type backgrounds) in *edm2–1*, *edm2–2, edm3–1* and *suvh456* plants at various sites surrounding the proximal *RPP7* polyadenylation site (Figure 6). Thus, levels of 2-phospho-serine RNAPII correlate well in the examined region with the levels of transcript expression, which are also higher in *edm2–1*, *edm2–2, edm3–1* and *suvh456* plants compared with their parental wild-type backgrounds (Figure 5b; Tsuchiya and Eulgem, 2013b). We also tested 2-phospho-serine RNAPII occupancy at *RPP7* exons 6 and 9, which are far downstream from the proximal polyadenylation site at *COPIA-R7*. However, levels of 2-phospho-serine RNAPII were undetectable in this part of the gene. This may reflect that transcript levels in these areas are very low, in both wild-type plants and the tested mutants (Figure 5b; Tsuchiya and Eulgem, 2013b). A mechanistic explanation for enhanced 2-phospho-serine RNAPII occupancy at the proximal *RPP7* polyadenylation site in *edm2–1*, *edm2–2, edm3–1* and *suvh456* plants may be pausing or slowing-down of transcription due to increased processing activity by the polyadenylation machinery at this site. More extensive use of the proximal polyadenylation site in these mutants may slow down the process of pre-mRNA synthesis resulting in greater density of 2-phospho-serine RNAPII.

DISCUSSION

Race-specific pathogen resistance is a particularly fascinating aspect of plant innate immunity. It requires fast generation of structural diversity among host NLR-receptor families, selection of NLR variants suitable for recognition of new pathogen challenges, and an evolutionary maturation process to equip useful NLR gene variants with a repertoire of regulatory mechanisms balancing their expression and optimizing their effectiveness. Unlike other biological non-self-recognition determinants, like T-cell receptors and antibodies, which are critical for the success of vertebrate immune systems and optimized by a somatic clonal selection process, new plant NLR variants do not develop within the life span of single organisms, but evolve over the course of generations. Yet, NLR evolution often can keep up with the fast pace of the evolution of AVR determinants in microbes despite the much longer generation times of plants. Besides catering the needs for structural innovation and balanced expression, fast NLR evolution also faces the challenge of equipping new immune receptors with efficient links to pre-existing defense signaling circuitry.

In this context it is remarkable that, in addition to numerous *rpp7* alleles, our extensive screens for *Hpa*-Hiks1 susceptible Col mutants uncovered only genes contributing to *RPP7* expression and protein stability. While SGT1b seems to control as a co-chaperone RPP7 protein stability, EDM2 and EDM3 participate in a mechanism controlling *RPP7* transcript processing, as does another component of the EDM2/EDM3 complex, the RRM-containing protein Anti-Silencing 1/Increase in Bonsai Methylation 2 (ASI1/IBM2; Saze *et al.*, 2013;

Wang *et al.*, 2013; Duan *et al.*, 2017). The fact that, at this point, the only single mutants found to strongly suppress *RPP7*-mediated immunity bear defects in regulators of this gene's expression and its product's stability highlights the importance of these steps as particularly critical for function of this NLR.

Similarly, complex mechanisms of regulation have been documented for other NLR genes, such as *SNC1*, the transcription of which is controlled by the activating histone marks H3K4me3 and H2Bub1, and seems to be counterbalanced by small RNA-mediated mechanisms (Li *et al.*, 2007; Yi and Richards, 2007; Xia *et al.*, 2013; Zou *et al.*, 2014). Alternative splicing has also been implicated in *SNC1* expression control (Xu *et al.*, 2012). Furthermore, SNC1 is negative regulated at the translational level (Wu *et al.*, 2017). Thus, *SNC1* regulation involves complex integration of various mechanisms of expression control operating at multiple levels.

RPP7 expression provides an example for a different control mechanism, which involves alternative transcript polyadenylation and is dependent on the transposon silencing mark H3K9me2. This mechanism has been recruited into the *RPP7* gene context by insertion of the *COPIA-R7* retrotransposon and is responsive to defense induction (Tsuchiya and Eulgem, 2013b). We previously showed that the histone-binding protein EDM2 is a key regulator of alternative polyadenylation at *RPP7*. Now, the map-based cloning of *EDM3/AIPP1* and characterization of loss-of-function mutants of this gene by our group and Duan *et al.* (2017) has implicated its product, an RRM domain-containing protein, as another regulator of RPP7 alternative polyadenylation. Importantly, Duan *et al.* (2017) demonstrated that EDM3/AIPP1 can bind to EDM2 along with another RRM-containing protein, ASI1/IBM2, and that both EDM3/AIPP1 and ASI1/IBM2 are necessary for production of full-length *RPP7* transcripts.

ASI1/IBM2 contains a Bromo-Adjacent Homology domain and, like EDM3, an RRM domain (Saze *et al.*, 2013; Wang *et al.*, 2013). Similar to EDM2, it was also shown to be required for the synthesis of full-length mRNAs at genes containing heterochromatic repeats/transposons within long introns. Loss of AS1/IBM2 function results in premature transcript termination at these heterochromatic regions. Besides *RPP7*, its targets include *IBM1.* The IBM1 histone H3 demethylase serves as a global anti-silencing factor suppressing in genic regions heterochromatin-associated marks, such as methylated cytosine in both CHG contexts as well as H3K9me2. As in the case of *RPP7*, expression of full-length IBM1 transcripts requires besides ASI1/IBM2 also EDM2 and EDM3/AIPP1 (Lei *et al.*, 2013; Saze *et al.*, 2013; Wang *et al.*, 2013; Duan *et al.*, 2017). Given the global anti-silencing function of IBM1, many of the effects observed in *asi1/ibm2*, *edm2* and *edm3/aipp1* mutants may be of indirect nature and dependent on IBM1.

Our experiments on *EDM3* extend the observations of Duan *et al.* (2017) in several respects. First, we illustrate the biological significance of *EDM3* by showing that an *edm3* loss of function mutant is fully susceptible to *Hpa*-Hiks1, but not other tested *Hpa* isolates. We also observed *Hpa*-Hiks1 susceptibility for an *asi1/ibm2* mutant (not shown); thus *EDM3/AIPP1* (as *EDM2* and likely *ASI1/IBM2*) are genetically essential for *RPP7*-mediated race-specific resistance. At a mechanistic level, we demonstrate a physical link between an H3K9me2/

chromatin-associated EDM2/EDM3 complex and *RPP7* mRNA, thereby extending our understanding of this unconventional mechanism of epigenetically controlled transcript processing. We showed by ChIP and RIP that under *in vivo* conditions both EDM2 and EDM3 are associated with H3K9me2-bearing *RPP7* chromatin and RNA templated by this genomic region. We could clearly localize these interactions to an area harboring the proximal polyadenylation site of *RPP7* at the 5'LTR of *COPIA-R7*.

Based on the observations, we propose the following explanation for molecular events controlling proximal polyadenylation of RPP7 transcripts: with its ability to bind to combinations of transcription-activating and -repressing histone marks (Tsuchiya and Eulgem, 2014), EDM2 is recruited and bound to chromatin at the border between *COPIA-R7* and the ECL-templating area in intron 1 of *RPP7*, which contains the proximal polyadenylation site. This area not only features high levels of the repressing mark H3K9me2, but also the activating marks H3K4me1 and H3K4me3 (Zhang *et al.*, 2009; Figure S4). EDM2 also promotes high levels of H3K9me2 in this area, as levels of this mark are reduced in *edm2* mutants (Tsuchiya and Eulgem, 2013b). It is unclear if EDM2 directly facilitates dimethylation of H3K9 or if, by binding to this mark, it simply protects it from being removed by other proteins (e.g. the H3K9 demethylase IBM1) as a consequence of active transcription in this area. In any case, by directly interacting with EDM3/AIPP1 (Duan *et al.*, 2017), EDM2 may help recruiting this RNA-binding protein to the area surrounding the proximal *RPP7* polyadenylation site. Association of both EDM2 and EDM3/AIPP1 with the nascent RNA in this area ties *RPP7* chromatin, EDM2, EDM3/AIPP1 and premature transcripts in this area into one complex. This is consistent with the association of both EDM2 and EDM3 with *RPP7* chromatin and transcripts we observed by ChIP and RIP (Figure 4). ASI1/IBM2 likely also resides in this complex, via binding to EDM3/AIPP1 and RPP7 pre-mRNA (Saze *et al.*, 2013; Wang *et al.*, 2013; Duan *et al.*, 2017).

While it is difficult to compare results based on different IP methods (ChIP and RIP) or results from the same IP method, but involving different antibodies/epitope pairs (anti-HA/HA-EDM2 versus anti-FLAG/EDM3-FLAG), it is remarkable that of all *in vivo* associations we examined by IP, the one between HA-EDM2 and transcripts bearing the 5' *COPIA-R7/RPP7* intron 1 border region is particularly pronounced (Figure 4). While this does not prove direct binding of EDM2 to RNA covering this region, it strongly implies a tight association. The EDM2 protein has an unusually complex architecture featuring, besides a histone H3-binding module of 2½ atypical PHD-fingers, the large uncharacterized ELP (EDM2-like proteins) domain with similarities to the active sites of prokaryotic N6-adenine methyltransferases (Eulgem *et al.*, 2007; Lei *et al.*, 2013; Tsuchiya and Eulgem, 2014). It has been proposed that EDM2 directly associates with RNA and methylates adenine at its 3'-end (Duan *et al.*, 2017), as this type of RNA methylation has recently been implicated in the 3'-end formation of plant mRNAs (Bodi *et al.*, 2012). While it is unclear how a role in 3'-end generation of transcripts can contribute to the suppression of proximal polyadenylation at *RPP7*, the proposed dual role of EDM2 as a factor interacting with both modified histone H3 and RNA is consistent with our results. RNA-binding proteins are known in many cases to associate with their targets as aggregates composed of multiple RNA-binding subunits, likely enhancing binding strength and specificity by binding

cooperatively (He *et al.*, 2016). Collectively, data from our studies and those of others suggest that they also likely apply to EDM2 together with ASI1/IBM2 and EDM3/AIPP1 (and possibly additional protein components) in the suppression of proximal transcript polyadenylation at *RPP7*. Future studies, including quantitative *in vitro* RNA-binding assays, will be needed to uncover molecular details of this interesting mechanism.

Our epigenome profiling analysis and that of others (Duan *et al.*, 2017) further imply that effects of EDM3/AIPP1 are not limited to *RPP7* and apply to a substantial portion of the Arabidopsis genome. However, in the vast majority of cases, EDM3 appears to serve as a suppressor of H3K9me2 and cytosine methylation. Besides *RPP7*, we found EDM3 only to promote H3K9me2 in three genes, none of which is an NLR gene. Thus, as in the case of EDM2 (Tsuchiya and Eulgem, 2013a), the effect of EDM3 on H3K9me2 levels seems to be context dependent. One possibility is that loci hypomethylated in the *edm3* mutant are direct targets (e.g. *RPP7*), while many of the hypermethylated loci may be indirect targets that may be secondarily affected by misregulation of *IBM1* in this mutant.

Proximal polyadenylation at *RPP7* is linked to the inclusion of an alternative exon (ECL exon 2; Figure 4a) into mature transcripts. It is unclear whether this alternative splice event is the cause or consequence of the early *RPP7* transcript termination. The inclusion of ECL exon 2 may cause early termination by retaining the proximal polyadenylation site in *RPP7* transcripts. Alternatively, choice of the proximal polyadenylation site by the polyadenylation machinery followed by transcript termination may determine the use of the ECL exon 2 splice acceptor site (and inclusion of this exon), because no alternative downstream splice acceptor sites are available. In any case, proximal *RPP7* transcript termination is likely based on the preferred choice of an upstream site (splice acceptor site or polyadenylation signal) over a downstream alternative. EDM2 and EDM3 (as well as ASI1/IBM2) suppress use of the upstream alternative, as loss of these regulators results in preferential proximal transcript termination.

Such alternative transcript-processing events have been associated with changes in RNAPII progression kinetics (Dujardin *et al.*, 2013; Kornblihtt *et al.*, 2013). Use of alternative upstream sites can slow down the process of pre-mRNA synthesis; presumably a consequence of the respective transcript-processing processes. Such a scenario is consistent with our observation of increased 2-phosphoserine RNAPII occupancy at the proximal *RPP7* polyadenylation site, which may reflect pausing or slowing-down of this enzyme in its progression along the DNA template. Additional studies will be required to shed light on the mechanistic details of the process of EDM2/EDM3-mediated and H3K9me2-dependent polyadenylation control we are describing here. In any case, EDM2 and EDM3 are critical parts of an innovative mechanism linking chromatin features to transcript processing.

EXPERIMENTAL PROCEDURES

Plant material and growth conditions

The Arabidopsis ecotype Columbia Col-0, Col-5 (*glabrous-1* mutant of Col-0), Duc1 and Ksk1 were obtained from the Arabidopsis Biological Resource Center (ABRC, Ohio State University). The *Hpa*-Hiks1 susceptible *rpp7–1* (Tör *et al.*, 2002), *edm2–1*, *edm2–2* (Eulgem

et al., 2007), *edm1* (Tör *et al.*, 2002) and Ws-*eds1* (Parker *et al.*, 1996) mutants have been described before. The Col-0 *suvh4/suvh5/suvh6* triple mutant (*suvh456*) was kindly provided by Dr Judith Bender (Brown University, Providence, RI, USA). As for *SGT1b/EDM1* and *EDM2* mapping (Tör *et al.*, 2002; Eulgem *et al.*, 2007), we used *Hpa*-Hiks1 susceptible F_2s from a cross of the *edm3–1* mutant (in Col-5 background) and wild-type Ler for mapping.

Map-based cloning of *EDM3*

Crude mapping of *EDM3* was performed using simple sequence length polymorphisms as described (Lukowitz *et al.*, 2000) with 278 *Hpa*-Hiks1 susceptible F_2s from crosses of *edm3–1* (in Col-5 background) to wild-type plants of the Ler accession. For variant analysis, Col-5 and *edm3–1* seedlings were grown on half-strength Murashige and Skoog (1/2 MS) solid medium containing 1% (w/v) sucrose in a growth chamber (16 h day, 8 h night, 22°C; 100 μE m^{-2} sec^{-1}) for 2 weeks. DNA from the aerial part of seedlings was isolated using DNeasy Plant Mini Kit (QIAGEN, Valencia, CA, USA). Sequencing libraries were prepared using NEBNext Ultra™ DNA library prep kit for Illumina (E7370; New England Biolabs, Ipswich, MA, USA) according to the manufacturer's instruction. Libraries were sequenced on the Illumina Miseq generating 2 × 300-bp pair-end sequence reads. Sequencing reads were mapped to the Arabidopsis genome (TAIR 10) using BWA (Burrows Wheeler Aligner) and the variants were identified by the SAMtools software (version 0.1.19).

Hyaloperonospora arabidopsidis infection and staining

The growth condition, propagation and application of *H. arabidopsidis* isolates *Hpa*-Hiks1, *Hpa*-Cala2 and *Hpa*-Cand5 were described previously (McDowell *et al.*, 2000). Two-week-old seedlings were spray-inoculated with spore suspensions (3–5 × 10^4 spores ml^{-1}) using Preval sprayers (Preval, Coal City, IL, USA). The extent of infections was determined at 7 dpi by counting visual sporangiophores or Trypan blue staining. Trypan blue staining was performed as previously described (McDowell *et al.*, 2000).

Transgenic lines

EDM3 genomic DNA preceded by either endogenous shorter or longer (117 or 834 bp) *EDM3* promoter stretches and followed by 550-bp genomic sequence downstream from the stop codon was cloned into pGWB1 using Gateway system (Invitrogen,Carlsbad, CA, USA) to yield *pE3s::E3g* or *pE3l::E3g*, respectively. Both vectors were introduced into *Agrobacterium tumefaciens* strain GV3101 and transformed into *edm3–1* plants by the floral dipping method (Clough and Bent, 1998). For functional complementation with FLAG-tagged EDM3, EDM3 genomic DNA driven by its endogenous shorter promoter was cloned into pEarleyGate302 vector (Earley *et al.*, 2006), and the resulting *pE3s::E3g-FLAG* vector was transformed into *edm3–1* as described above. For complementation of EDM3 driven by *CaMV35S* promoter, two EDM3 full-length cDNA isoforms were first amplified by PCR-driven overlap extension (Heckman and Pease, 2007), and then introduced into either pEarleyGate202 vector (FLAG-tagged) or pMDC43 (GFP-tagged) resulting in *p35S::FLAG-E3cds-1/−2* or *p2x35S::GFP-E3cds-1/−2*, respectively (Curtis and Grossniklaus, 2003; Earley *et al.*, 2006). T_3 homozygous plants with a single insertion locus were used for experiments. All the primers used are listed in Table S5.

Microscopy

Fluorescence was visualized using a Leica SP5 confocal microscope. Leaves were infiltrated with 1 μg ml^{-1} of 4',6-diamidino-2-phenylindole solution prior to imaging.

RNA isolation and qRT-PCR analysis

Aerial parts of 2-week-old plants were harvested from 1/2 MS solid plates and used for total RNAs isolation. Total RNA was isolated using TRIzol reagent (Life Technologies, Invitrogen) and treated with TURBO DNA-free™ kit (Ambion, Life Technologies, Invitrogen). Reverse transcription was conducted by Maxima reverse transcriptase (Thermo Fisher Scientific, Waltham, MA, USA) with 100 pmol of oligo $(dT)_{18}$ primers. Real-time RT-PCR was performed with the CFX Connect detection system (Bio-Rad) using iQ SYBR Green Supermix (Bio-Rad, Hercules, CA, USA). All the primers used for qRT-PCR are listed in Table S5.

Chromatin immunoprecipitation

Aerial parts of 2-week-old plants were harvested from 1/2 MS solid plates and used for ChIP assays. ChIP was performed as described previously (Tsuchiya and Eulgem, 2013b) using anti-H3K9me2 (ab1220, Abcam, Cambridge, MA, USA), anti-H3 C-terminal (61277; Active Motif, Carlsbad, CA, USA), anti-FLAG M2 affinity gel (A2220, Sigma-Aldrich, St. Louis, MO, USA), RNAPII-S2 (Millipore, Temecula, CA, USA, 04–1571) and anti-HA (AB9110, Abcam) antibodied. All primers used for ChIP-qPCR are listed in Table S5.

RNA immunoprecipitation

Aerial parts of 2-week-old plants were harvested from 1/2 MS solid plates and used for RIP assays. Chromatin-RNA complexes isolation was performed as described for ChIP previously (Tsuchiya and Eulgem, 2013b) with several modifications. Briefly, 1 g of aerial parts of 2-week-old plants was harvested and fixed in cross-linking buffer (1% formaldehyde, 1 mM phenylmethylsulfonyl fluoride (PMSF) in PBS buffer, pH 7.4) for 12 min at room temperature under vacuuming. Cross-linking was quenched with 0.125 M glycine, and the materials were washed three times with water, dried with towels, frozen and stored at −80°C until use. Chromatin was extracted by grinding fixed tissues to powder in liquid N_2, followed by homogenization in nuclei isolation buffer [0.25 M sucrose, 15 m M Pipes (pH 6.8), 5 mM $MgCl_2$, 60 mM KCl, 15 mM NaCl, 1 mM $CaCl_2$, 0.9% Triton X-100, 1 mM PMSF, 1% proteinase inhibitor mixture for plant cell and tissue extracts (Sigma-Aldrich, 8 U ml^{-1} Ribolock RNase Inhibitor (Thermo Fisher Scientific]. The homogenate was filtered through two layers of miracloth, and the filtrate was centrifuged for 20 min at 11 000 ***g***. The pellet was resuspended in nuclei lysis buffer [50 mM Hepes (pH 7.5), 150 mM NaCl, 10 mM EDTA, 1% sodium dodecyl sulfate (SDS), 0.1% sodium deoxycholate, 1% Triton X-100, 1% proteinase inhibitor mixture, 160 U ml^{-1} Ribolock RNase Inhibitor]. The extracted protein–RNA was sheared by sonication to approximately 350–1000-bp fragments and centrifuged.

For ChIP, chromatin diluted with ChIP dilution buffer [50 mM Hepes (pH 7.5), 150 mM NaCl, 1 mM EDTA, 0.1% sodium deoxycholate, 1% Triton X-100, 1% proteinase inhibitor

mixture, 160 U ml^{-1} Ribolock RNase Inhibitor] was precleared with 60 µl of Protein A-agarose (Roche, Branford, CT, USA) for 1 h at 4°C. A fraction of the supernatants was saved and, after cross-linking, TURBO DNA-freeTM kit treatment and reverse transcription was used as input control in qRT-PCR measurement. The precleared protein–RNA complex was immunoprecipitated overnight at 4°C with Protein A-agarose bound by anti-HA antibody or anti-FLAG M2 affinity gel. After incubation, the beads were washed six times with wash buffer [20 mM Tris-HCl (pH 8.0), 150 mM NaCl, 5 mM $MgCl_2$, 0.5% Nonidet P-40, 5 mM dithiothreitol, protease inhibitor cocktail tablets (Complete Mini, Roche), 40 U ml^{-1} Ribolock RNase Inhibitor] and twice with TE buffer [10 mM Tris-HCl (pH 8.0), 1 mM EDTA]; Elution buffer (100 mM Tris-HCl, pH 8.0, 10 mM EDTA, 1% SDS, 800 U ml^{-1} Ribolock RNase Inhibitor) was added to individual samples and incubated for 10 min at room temperature. Reverse crosslinking was performed by adding 0.3 M NaCl and 2 µg of proteinase K for 1 h at 65°C. RNA was isolated using TRIzol reagent and treated with TURBO DNA-freeTM kit (Ambion). Reverse transcription was conducted by Maxima reverse transcriptase (Thermo Scientific) with 100 pmol Random Hexamers (Invitrogen). Reverse transcription for No-RT controls was also performed with the same condition without adding Maxima Reverse Transcriptase. qRT-PCR was performed with the CFX Connect detection system (Bio-Rad) using iQ SYBR Green Supermix (Bio-Rad). All the primers used for qRT-PCR are listed in Table S5.

H3K9me2 ChIP-seq and data analysis

Chromatin immunoprecipitation-seq libraries were prepared using NEBNext Ultra™ II DNA library prep kit for Illumina (E7645; New England Biolabs) according to the manufacturer's instruction. Libraries were sequenced on the Illumina NextSeq500 generating 75-bp signal-end sequence reads.

For each Chip-Seq library, raw reads quality was first analyzed using FastQC (https://www.bioinformatics.babraham.ac.uk/projects/fastqc/), and any base with a quality score below 25 or N was trimmed using Sickle (https://github.com/najoshi/sickle). Trimmed reads were then mapped to the *A. thaliana* genome (TAIR 10) using BWA 0.7.15-r1140 with mem option default parameters (Li and Durbin, 2009; see Table S6 for mapping statistics). Uniquely mapped reads were further filtered for calculating H3K9me2 coverage in transcripts, while unfiltered reads were used for calculating H3K9me2 coverage in TEs. The number of reads mapped to each transcript was determined using BEDTools v2.25.0 (Quinlan and Hall, 2010), and Spearman correlation coefficients were calculated between biological replicates. To compare H3K9me2 level between Col-5 and *edm3–1* samples, no expressed transcripts with coverage value below 1 in all libraries were removed. Transcripts representing differentially methylated regions were determined using DEseq2 in R (Love *et al.*, 2014) with a *P*-adjusted value of 0.05 and a 1.2-fold change. For genome browser tracks, read coverage per nucleotide was calculated using BEDTools. Coverage values were then normalized per million mapped reads for each library.

The Gene Expression Omnibus accession number for ChIP-seq and variant analysis sequencing data reported in this study is GSE108490.

RNA-seq data analysis

EDM3 RNA-seq data were obtained from Duan *et al.* (2017) with the following accession numbers: SRR5515902, SRR5515903, SRR5515906 and SRR5515907. Differentially expressed transcripts were determined using DEseq2 (Love *et al.*, 2014) with a *P*-adjusted value of 0.05 and a 1.2-fold change.

Supplementary Material

Refer to Web version on PubMed Central for supplementary material.

ACKNOWLEDGEMENTS

The authors thank Dr Jeffery L. Dangl (University of North Carolina, USA) for guidance and support during early stages of this project, critical reading of this manuscript and helpful discussions. The authors also thank Dr Artur Jarmołowski (Adam Mickiewicz University, Poznan, Poland) for helpful discussions and advice. The authors thank Dr Craig S. Pikaard (Department of Biology, Indiana University, Bloomington, Indiana, USA) for pEarleyGate vectors; Dr Mark D. Curtis (Institute of Plant Biology and Zürich-Basel Plant Science Center, University of Zürich, Zürich, Switzerland) for pMDC vectors; Dr Judith Bender (Brown University, Providence, RI, USA) for providing the *suvh456* mutant. EH and AC were supported by grants from the Biotechnology and Biological Science Research Council (207/ICR07554 and a training grant for AC). This work was further supported by the US National Science Foundation (NSF) grant IOS-1457329 to TE. The authors thank the NSF-supported SIGNAL T-DNA Express and NSF-supported Arabidopsis Biological Resource Center for providing seeds. The authors wish to dedicate this paper to the occasion of Jeffery L. Dangl's 61st birthday on 13 October 2018.

REFERENCES

Abramovitch RB, Anderson JC and Martin GB (2006) Bacterial elicitation and evasion of plant innate immunity. Nat. Rev. Mol. Cell Biol 7, 601–611. [PubMed: 16936700]

Allen RL, Bittner-Eddy PD, Grenville-Briggs LJ, Meitz JC, Rehmany AP, Rose LE and Beynon JL (2004) Host-parasite coevolutionary conflict between Arabidopsis and downy mildew. Science 306, 1957–1960. [PubMed: 15591208]

Anderson RG, Deb D, Fedkenheuer K and McDowell JM (2015) Recent progress in RXLR effector research. Mol. Plant Microbe Interact 28, 1063–1072. [PubMed: 26125490]

Bernatavichute YV, Zhang X, Cokus S, Pellegrini M and Jacobsen SE (2008) Genome-wide association of histone H3 lysine nine methylation with CHG DNA methylation in *Arabidopsis thaliana*. PLoS One 3, e3156. [PubMed: 18776934]

Bieri S, Mauch S, Shen QH et al. (2004) RAR1 positively controls steady state levels of barley MLA resistance proteins and enables sufficient MLA6 accumulation for effective resistance. Plant Cell 16, 3480–3495. [PubMed: 15548741]

van der Biezen EA, Freddie CT, Kahn K, Parker JE and Jones JDG (2002) Arabidopsis *RPP4* is a member of the *RPP5* multigene family of TIR-NB-LRR genes and confers downy mildew resistance through multiple signaling components. Plant J 29, 439–451. [PubMed: 11846877]

Bittner-Eddy P, Can C, Gunn N, Pinel M, Tor M, Crute I, Holub EB and Beynon J (1999) Genetic and physical mapping of the RPP13 locus, in Arabidopsis, responsible for specific recognition of several Peronospora parasitica (downy mildew) isolates. Mol. Plant Microbe Interact 12, 792–802. [PubMed: 10494631]

Bodi Z, Zhong S, Mehra S, Song J, Graham N, Li H, May S and Fray RG (2012) Adenosine methylation in Arabidopsis mRNA is associated with the 3' end and reduced levels cause developmental defects. Front. Plant Sci 3, 48. [PubMed: 22639649]

Bomblies K and Weigel D (2007) Hybrid necrosis: autoimmunity as a potential gene-flow barrier in plant species. Nat. Rev. Genet 8, 382–393. [PubMed: 17404584]

Bomblies K, Lempe J, Epple P, Warthmann N, Lanz C, Dangl JL and Weigel D (2007) Autoimmune response as a mechanism for a Dobzhansky-Muller-type incompatibility syndrome in plants. PLoS Biol 5, e236. [PubMed: 17803357]

Cheng YT, Li Y, Huang S, Huang Y, Dong X, Zhang Y and Li X (2011) Stability of plant immune-receptor resistance proteins is controlled by SKP1-CULLIN1-F-box (SCF)-mediated protein degradation. Proc. Natl Acad. Sci. USA 108, 14 694–14 699.

Chisholm ST, Coaker G, Day B and Staskawicz BJ (2006) Host-microbe interactions: shaping the evolution of the plant immune response. Cell 124, 803–814. [PubMed: 16497589]

Clough SJ and Bent AF (1998) Floral dip: a simplified method for Agrobacterium-mediated transformation of *Arabidopsis thaliana*. Plant J 16, 735–743. [PubMed: 10069079]

Curtis MD and Grossniklaus U (2003) A gateway cloning vector set for high-throughput functional analysis of genes in planta. Plant Physiol 133, 462–469. [PubMed: 14555774]

Dangl JL and McDowell JM (2006) Two modes of pathogen recognition by plants. Proc. Natl Acad. Sci. USA 103, 8575–8576. [PubMed: 16735473]

Duan CG, Wang X, Zhang L et al. (2017) A protein complex regulates RNA processing of intronic heterochromatin-containing genes in Arabidopsis. Proc. Natl Acad. Sci. USA 114, E7377–E7384. [PubMed: 28808009]

Dujardin G, Lafaille C, Petrillo E et al. (2013) Transcriptional elongation and alternative splicing. Biochim. Biophys. Acta 1829, 134–140. [PubMed: 22975042]

Earley KW, Haag JR, Pontes O, Opper K, Juehne T, Song K and Pikaard CS (2006) Gateway-compatible vectors for plant functional genomics and proteomics. Plant J 45, 616–629. [PubMed: 16441352]

Eulgem T, Tsuchiya T, Wang X, Cuzick A, Beasley B, Toer M, McDowell JM, Holub E, Zhu T and Dangl JL (2007) EDM2 is required for *RPP7*-dependent disease resistance in Arabidopsis and affects *RPP7* transcript levels. Plant J 49, 829–839. [PubMed: 17253987]

Flor HH (1971) Current status of the gene-for-gene concept. Annu. Rev. Phytopathol 9, 275–296.

He C, Sidoli S, Warneford-Thomson R, Tatomer DC, Wilusz JE, Garcia BA and Bonasio R (2016) High-resolution mapping of RNA-binding regions in the nuclear proteome of embryonic stem cells. Mol. Cell 64, 416–430. [PubMed: 27768875]

Heckman KL and Pease LR (2007) Gene splicing and mutagenesis by PCR-driven overlap extension. Nat. Protoc 2, 924–932. [PubMed: 17446874]

Holt BF III, Belkhadir Y and Dangl JL (2005) Antagonistic control of disease resistance protein stability in the plant immune system. Science 309, 929–932. [PubMed: 15976272]

Holub EB (2001) The arms race is ancient history in Arabidopsis, the wild-flower. Nat. Rev. Genet 2, 1–12.

Holub EB (2008) Natural history of *Arabidopsis thaliana* and oomycete symbioses. Eur. J. Plant Pathol 122, 91–109.

Holub EB, Beynon JL and Ctute IR (1994) Phenotypic and genotypic characterization of interactions between isolates of *Peronospora parasitica* and accessions of *Arabidopsis thaliana*. Mol. Plant Microbe Interact 7, 223–239.

Hubert DA, Tornero P, Belkhadir Y, Krishna P, Takahashi A, Shirasu K and Dangl JL (2003) Cytosolic HSP90 associates with and modulates the Arabidopsis RPM1 disease resistance protein. EMBO J 22, 5679–5689. [PubMed: 14592967]

Jacob F, Vernaldi S and Maekawa T (2013) Evolution and conservation of plant NLR functions. Front. Immunol 4, 297. [PubMed: 24093022]

Jones JD, Vance RE and Dangl JL (2016) Intracellular innate immune surveillance devices in plants and animals. Science 354, aaf6395. [PubMed: 27934708]

Karasov TL, Kniskern JM, Gao L et al. (2014) The long-term maintenance of a resistance polymorphism through diffuse interactions. Nature 512, 436–440. [PubMed: 25043057]

Kornblihtt AR, Schor IE, Allo M, Dujardin G, Petrillo E and Munoz MJ (2013) Alternative splicing: a pivotal step between eukaryotic transcription and translation. Nat. Rev. Mol. Cell Biol 14, 153–165. [PubMed: 23385723]

Korves T and Bergelson J (2004) A novel cost of *R* gene resistance in the presence of disease. Am. Nat 163, 489–504. [PubMed: 15122498]

Lai Y and Eulgem T (2017) Transcript-level expression control of plant NLR genes. Mol. Plant Pathol 19, 1267–1281. [PubMed: 28834153]

Lei M, La H, Lu K et al. (2013) Arabidopsis EDM2 promotes *IBM1* distal polyadenylation and regulates genome DNA methylation patterns. Proc. Natl Acad. Sci. USA 111, 527–532. [PubMed: 24248388]

Li H and Durbin R (2009) Fast and accurate short read alignment with Burrows-Wheeler transform. Bioinformatics 25, 1754–1760. [PubMed: 19451168]

Li Y, Yang S, Yang H and Hua J (2007) The TIR-NB-LRR gene *SNC1* is regulated at the transcript level by multiple factors. Mol. Plant Microbe Interact 20, 1449–1456. [PubMed: 17977156]

Li X, Kapos P and Zhang Y (2015) NLRs in plants. Curr. Opin. Immunol 32, 114–121. [PubMed: 25667191]

Love MI, Huber W and Anders S (2014) Moderated estimation of fold change and dispersion for RNA-seq data with DESeq2. Genome Biol 15, 550. [PubMed: 25516281]

Lukowitz W, Gillmour CS and Scheible W-R (2000) Positional cloning in Arabidopsis: why it feels good to have a genome initiative working for you. Plant Physiol 123, 795–806. [PubMed: 10889228]

Mackey D, Belkhadir Y, Alonso JM, Ecker JR and Dangl JL (2003) Arabidopsis RIN4 is a target of the type III virulence effector AvrRpt2 and modulates RPS2-mediated resistance. Cell 112, 379–389. [PubMed: 12581527]

McDowell JM, Dhandaydham M, Long TA, Aarts MGM, Goff S, Holub EB and Dangl JL (1998) Intragenic recombination and diversifying selection contribute to the evolution of downy mildew resistance at the *RPP8* locus of Arabidopsis. Plant Cell 10, 1861–1874. [PubMed: 9811794]

McDowell JM, Cuzick A, Can C, Beynon J, Dangl JL and Holub EB (2000) Downy mildew (Peronospora parasitica) resistance genes in Arabidopsis vary in functional requirements for NDR1, EDS1, NPR1, and salicylic acid accumulation. Plant J 22, 523–530. [PubMed: 10886772]

Meyers BC, Kozik A, Griego A, Kuang H and Michelmore RW (2003) Genome-wide analysis of NBS-LRR-encoding genes in Arabidopsis. Plant Cell 15, 809–834. [PubMed: 12671079]

Mohr TJ, Mammarella ND, Hoff T, Woffenden BJ, Jelesko JG and McDowell JM (2010) The Arabidopsis downy mildew resistance gene *RPP8* is induced by pathogens and salicylic acid and is regulated by W box *cis* elements. Mol. Plant Microbe Interact 23, 1303–1315. [PubMed: 20831409]

Palma K, Thorgrimsen S, Malinovsky FG, Fiil BK, Nielsen HB, Brodersen P, Hofius D, Petersen M and Mundy J (2010) Autoimmunity in Arabidopsis acd11 is mediated by epigenetic regulation of an immune receptor. PLoS Pathog 6, e1001137. [PubMed: 20949080]

Parker JE, Holub EB, Frost LN, Falk A, Gunn ND and Daniels MJ (1996) Characterization of *eds1*, a mutation in Arabidopsis suppressing resistance to *Peronospora parasitica* specified by several different *RPP* genes. Plant Cell 8, 2033–2046. [PubMed: 8953768]

Quinlan AR and Hall IM (2010) BEDTools: a flexible suite of utilities for comparing genomic features. Bioinformatics 26, 841–842. [PubMed: 20110278]

Reignault P, Frost LN, Richardson H, Daniels MJ, Jones JDG and Parker JE (1996) Four *Arabidopsis RPP* loci controlling resistance to the *Noco2* isolate of *Peronospora parasitica* map to regions known to contain other *RPP* recognition specificities. Mol. Plant Microbe Interact 9, 464–473. [PubMed: 8755623]

Saze H, Kitayama J, Takashima K, Miura S, Harukawa Y, Ito T and Kakutani T (2013) Mechanism for full-length RNA processing of Arabidopsis genes containing intragenic heterochromatin. Nat. Commun 4, 2301. [PubMed: 23934508]

Schulze-Lefert P (2004) Plant immunity: the origami of receptor activation. Curr. Biol 14, R22–R24. [PubMed: 14711430]

Shirano Y, Kachroo P, Shah J and Klessig DF (2002) A gain-of-function mutation in an Arabidopsis Toll interleukin1 receptor-nucleotide binding site-leucine-rich repeat type R gene triggers defense responses and results in enhanced disease resistance. Plant Cell 14, 3149–3162. [PubMed: 12468733]

Sinapidou E, Williams K, Nott L, Bahkt S, Tor M, Crute I, Bittner-Eddy P and Beynon J (2004) Two TIR:NB:LRR genes are required to specify resistance to Peronospora parasitica isolate Cala2 in Arabidopsis. Plant J 38, 898–909. [PubMed: 15165183]

Stokes TL, Kunkel BN and Richards EJ (2002) Epigenetic variation in Arabidopsis disease resistance. Genes Dev 16, 171–182. [PubMed: 11799061]

Tian D, Traw MB, Chen JQ, Kreitman M and Bergelson J (2003) Fitness costs of R-gene-mediated resistance in *Arabidopsis thaliana*. Nature 423, 74–77. [PubMed: 12721627]

Tör M, Holub EB, Brose E, Musker R, Gunn N, Can C, Crute IR and Beynon JL (1994) Map positions of three loci in *Arbaidopsis thaliana* associated with isolate-specific recognition of *Peronospora parasitica*. Mol. Plant Microbe Interact 7, 214–222.

Tör M, Gordon P, Cuzick A, Eulgem T, Sinapidou E, Mert-Turk F, Can C, Dangl JL and Holub EB (2002) Arabidopsis SGT1b is required for defense signaling conferred by several downy mildew resistance genes. Plant Cell 14, 993–1003. [PubMed: 12034892]

Tsuchiya T and Eulgem T (2010a) The Arabidopsis defense component EDM2 affects the floral transition in an FLC-dependent manner. Plant J 62, 518–528. [PubMed: 20149132]

Tsuchiya T and Eulgem T (2010b) Co-option of EDM2 to distinct regulatory modules in *Arabidopsis thaliana* development. BMC Plant Biol 10, 203. [PubMed: 20840782]

Tsuchiya T and Eulgem T (2011) *EMSY*-like genes are required for full *RPP7*-mediated race-specific immunity and basal defense in Arabidopsis. Mol. Plant Microbe Interact 24, 1573–1581. [PubMed: 21830950]

Tsuchiya T and Eulgem T (2013a) Mutations in *EDM2* selectively affect silencing states of transposons and induce plant developmental plasticity. Sci. Rep 3, 1701. [PubMed: 23609044]

Tsuchiya T and Eulgem T (2013b) An alternative polyadenylation mechanism coopted to the Arabidopsis *RPP7* gene through intronic retrotransposon domestication. Proc. Natl Acad. Sci. USA 110, E3535–E3543. [PubMed: 23940361]

Tsuchiya T and Eulgem T (2014) The PHD-finger module of the *Arabidopsis thaliana* defense regulator EDM2 can recognize triply modified histone H3 peptides. Plant Signal. Behav 9, e29202. [PubMed: 25763495]

Wang R and Brattain MG (2007) The maximal size of protein to diffuse through the nuclear pore is larger than 60 kDa. FEBS Lett 581, 3164–3170. [PubMed: 17588566]

Wang X, Duan CG, Tang K et al. (2013) RNA-binding protein regulates plant DNA methylation by controlling mRNA processing at the intronic heterochromatin-containing gene IBM1. Proc. Natl Acad. Sci. USA 110, 15 467–15 472.

Wu Z, Huang S, Zhang X, Wu D, Xia S and Li X (2017) Regulation of plant immune receptor accumulation through translational repression by a glycine-tyrosine-phenylalanine (GYF) domain protein. Elife 6, e23684. [PubMed: 28362261]

Xia S, Cheng YT, Huang S et al. (2013) Regulation of transcription of nucleotide-binding leucine-rich repeat-encoding genes *SNC1* and *RPP4* via H3K4 trimethylation. Plant Physiol 162, 1694–1705. [PubMed: 23690534]

Xiao S, Brown S, Patrick E, Brearley C and Turner JG (2003) Enhanced transcription of the Arabidopsis disease resistance genes *RPW8.1* and *RPW8.2* via a salicylic acid-dependent amplification circuit is required for hypersensitive cell death. Plant Cell 15, 33–45. [PubMed: 12509520]

Xu F, Xu S, Wiermer M, Zhang Y and Li X (2012) The cyclin L homolog MOS12 and the MOS4-associated complex are required for the proper splicing of plant resistance genes. Plant J 70, 916–928. [PubMed: 22248079]

Yi H and Richards EJ (2007) A cluster of disease resistance genes in Arabidopsis is coordinately regulated by transcriptional activation and RNA silencing. Plant Cell 19, 2929–2939. [PubMed: 17890374]

Zhang X, Bernatavichute YV, Cokus S, Pellegrini M and Jacobsen SE (2009) Genome-wide analysis of mono-, di-and trimethylation of histone H3 lysine 4 in *Arabidopsis thaliana*. Genome Biol 10, R62. [PubMed: 19508735]

Zou B, Yang DL, Shi Z, Dong H and Hua J (2014) Monoubiquitination of histone 2B at the disease resistance gene locus regulates its expression and impacts immune responses in Arabidopsis. Plant Physiol 165, 309–318. [PubMed: 24664204]

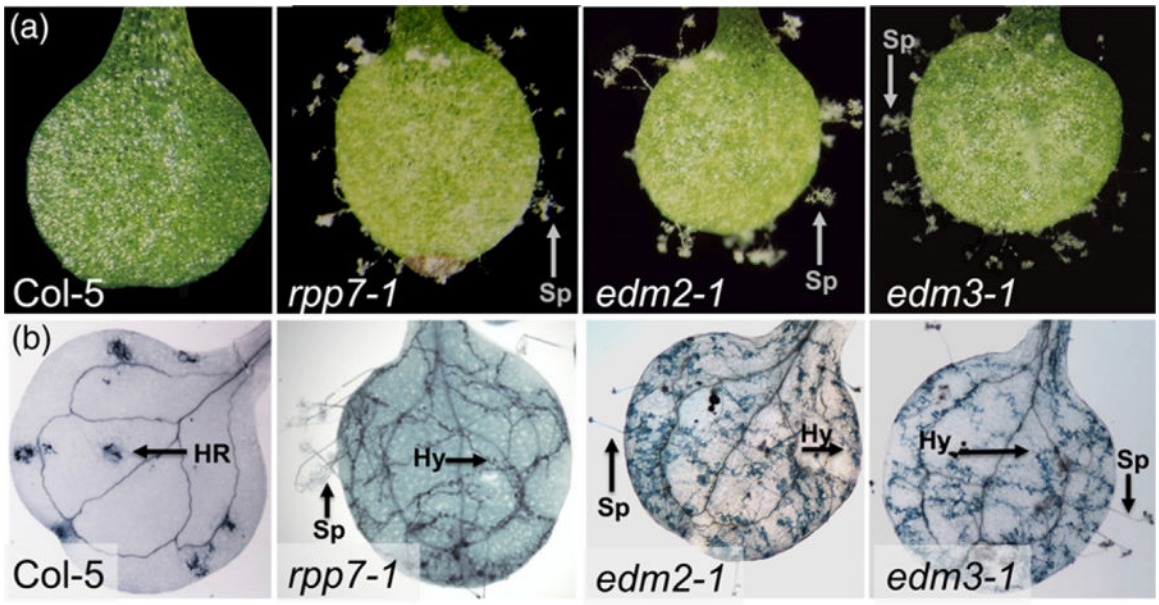

Figure 1.

The *Hpa*-Hiks1 susceptibility phenotype of the *edm3–1* mutant resembles that of the *rpp7* and *edm2* mutants.

(a) Cotyledons of wild-type and mutant lines of the Col-5 accession 7 days post-infection (dpi) with *Hpa*-Hiks1. The *rpp7–1*, *edm2–1* and *edm3–1* mutants exhibit high levels of *Hyaloperonospora arabidopsidis* sporulation.

(b) Trypan blue-stained cotyledons of the same lines shown in (a) 7 dpi with *Hpa*-Hiks1. Arrows are pointing to characteristic features. HR, hypersensitive response-associated cell death; Sp, *H. arabidopsidis* sporangiophore; Hy, *H. arabidopsidis* hyphae.

(a, b) shown are typical results.

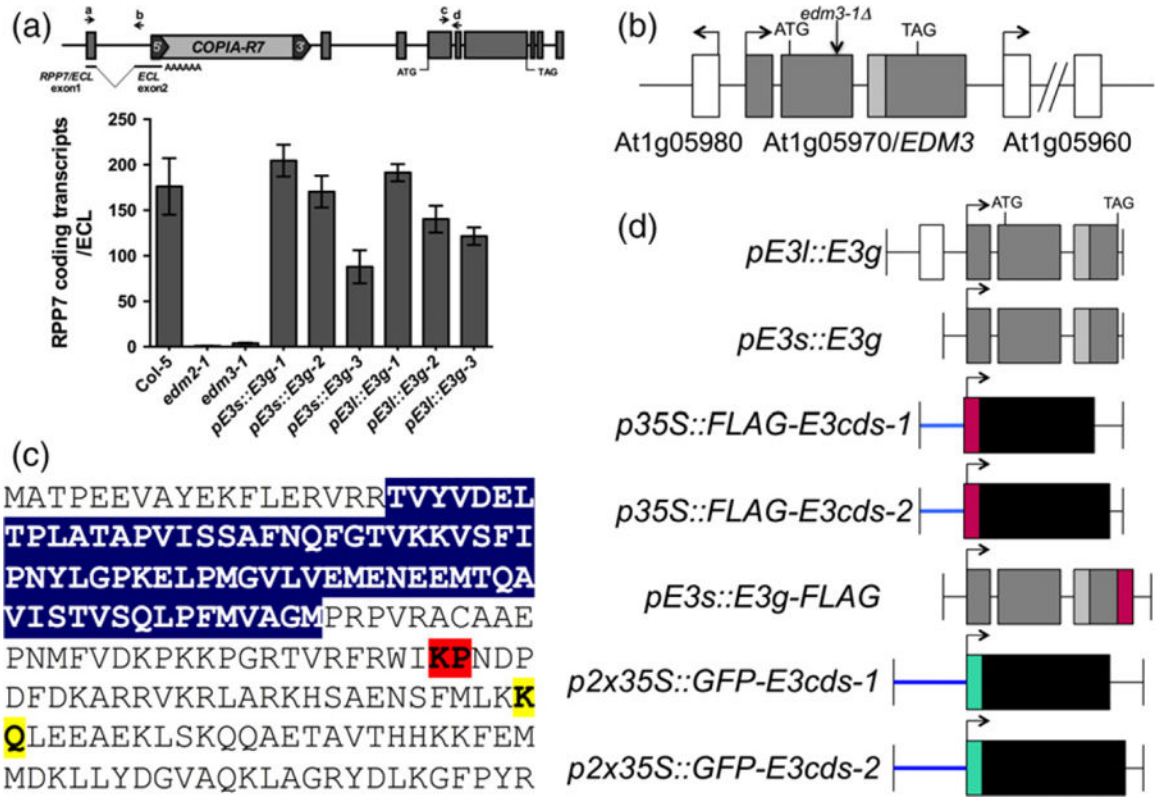

Figure 2.

EDM3 is At1g05970 and encodes an RNA recognition motif (RRM) domain protein.

(a) Ratios of RPP7 full-length coding transcripts and the proximal-polyadenylated non-coding ECL transcript determined by quantitative real-time-polymerase chain reaction (qRT-PCR). Schematic representation of the *RPP7* area studied in experiments. Arrows represent regions amplified by qRT-PCR shown below (primers a and b for ECL transcripts; primers c and d for RPP7 coding transcripts). *pE3s::E3g-1*, *−2, −3* and *pE3l::E3g-1*, *−2, −3* are complementation lines expressing in the *edm3–1* background EDM3 driven by either the endogenous shorter or longer EDM3 promoter (117 or 834 bp, respectively; see also panel d of this figure).

(b) Annotation of genomic region at At1g05970/*EDM3*.

(c) Amino acid sequence of proteins encoded by At1g05970/*EDM3*. Blue: RRM domain; red: amino acids deleted in both isoforms encoded in *edm3–1* mutant; yellow: amino acids present in EDM3 isoform 2, but not isoform 1, due to alternative splicing.

(d) Constructs used in transgenic *edm3–1* plants for functional complementation and other experiments described in this article. *pE3l*: endogenous upstream intergenic sequence comprising 834 bp upstream from predicted At1g05970 transcription start site (TSS); *pE3s*: endogenous upstream intergenic sequence comprising 117 bp upstream from predicted At1g05970 TSS until next upstream gene; *p35S*: *CaMV35S* promoter; *p2x35S*: promoter consisting of two tandem copies of *CaMV35S* enhancer; *E3g*: At1g05970 genomic sequence comprising stretch from TSS until polyadenylation signal until stop codon; *E3cds-1*: coding sequence of spliceform 1 of At1g05970; *E3cds-2*: coding sequence of spliceform 2 of At1g05970; *FLAG*: coding sequence of FLAG-epitope tag fused in frame to At1g05970

coding sequence; *GFP*: coding sequence of green fluorescent protein fused in frame to At1g05970 coding sequence; (b, d) horizontal arrow symbol; TSS pointing in direction of arrow; white boxes: exons of genes in vicinity of At1g05970; dark gray boxes: exonic sequences common to both At1g05970 splice forms; light gray boxes: exonic sequence specific for At1g05970 splice form 2; black boxes: cDNA sequences representing the short or long EDM3 transcript isoforms; red box: sequence encoding FLAG tag; green box: sequence encoding GFP.

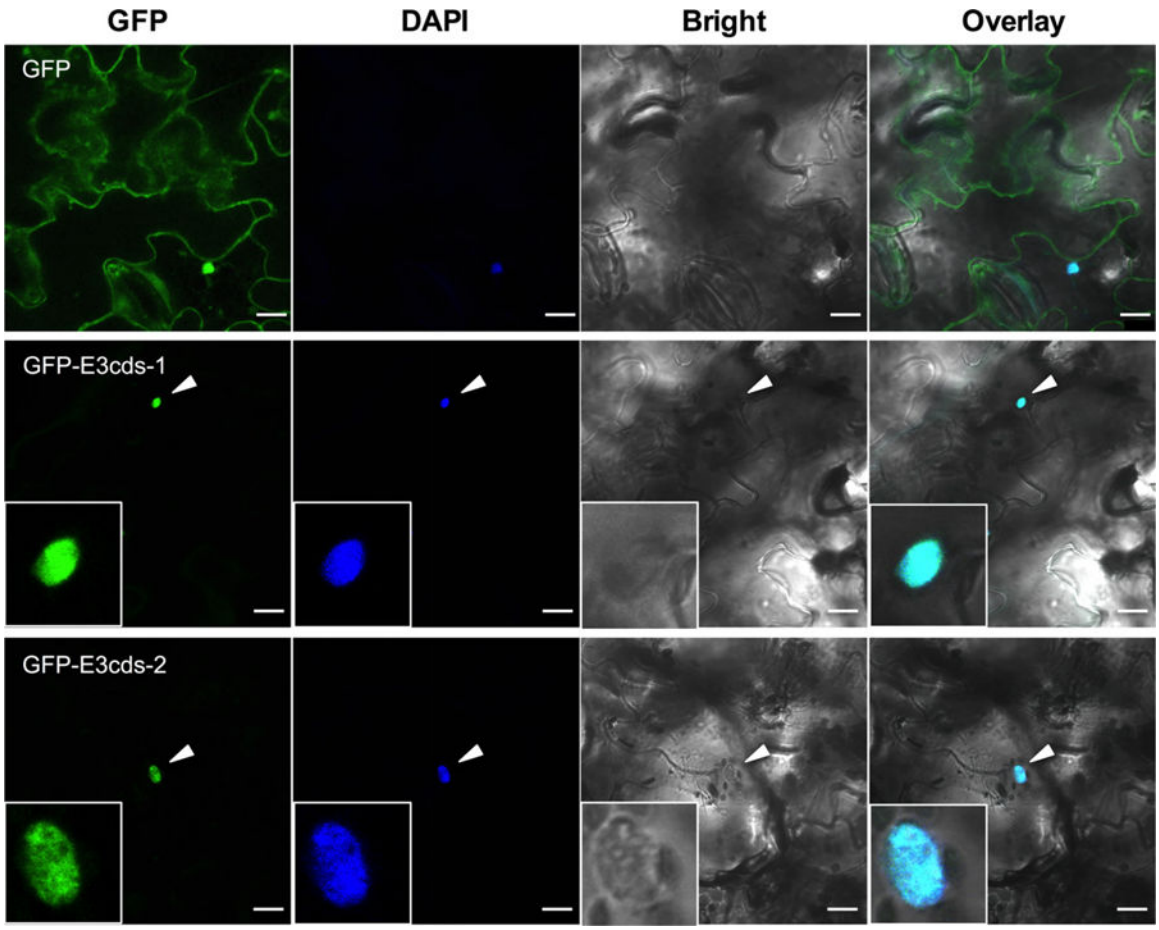

Figure 3.

Subcellular localization of EDM3 isoforms.

Confocal microscopy images of tissues from transgenic Col-0 plants expressing a *CaMV35S*-promoter::GFP construct (GFP) or transgenic *edm3–1* plants expressing the *p2X35S::GFP-E3cds-1* (GFP-E3cds-1) or *p2X35S::GFP-E3cds-2* (GFP-E3cds-2) constructs (see also Figure 2d). White arrowheads point to nuclear regions. Scale bar: 10 lM. Selected GFP-fluorescing nuclei are shown enlarged in white-framed squares in the lower left corners of some panels. Overlay: merged GFP, DAPI and bright-field images.

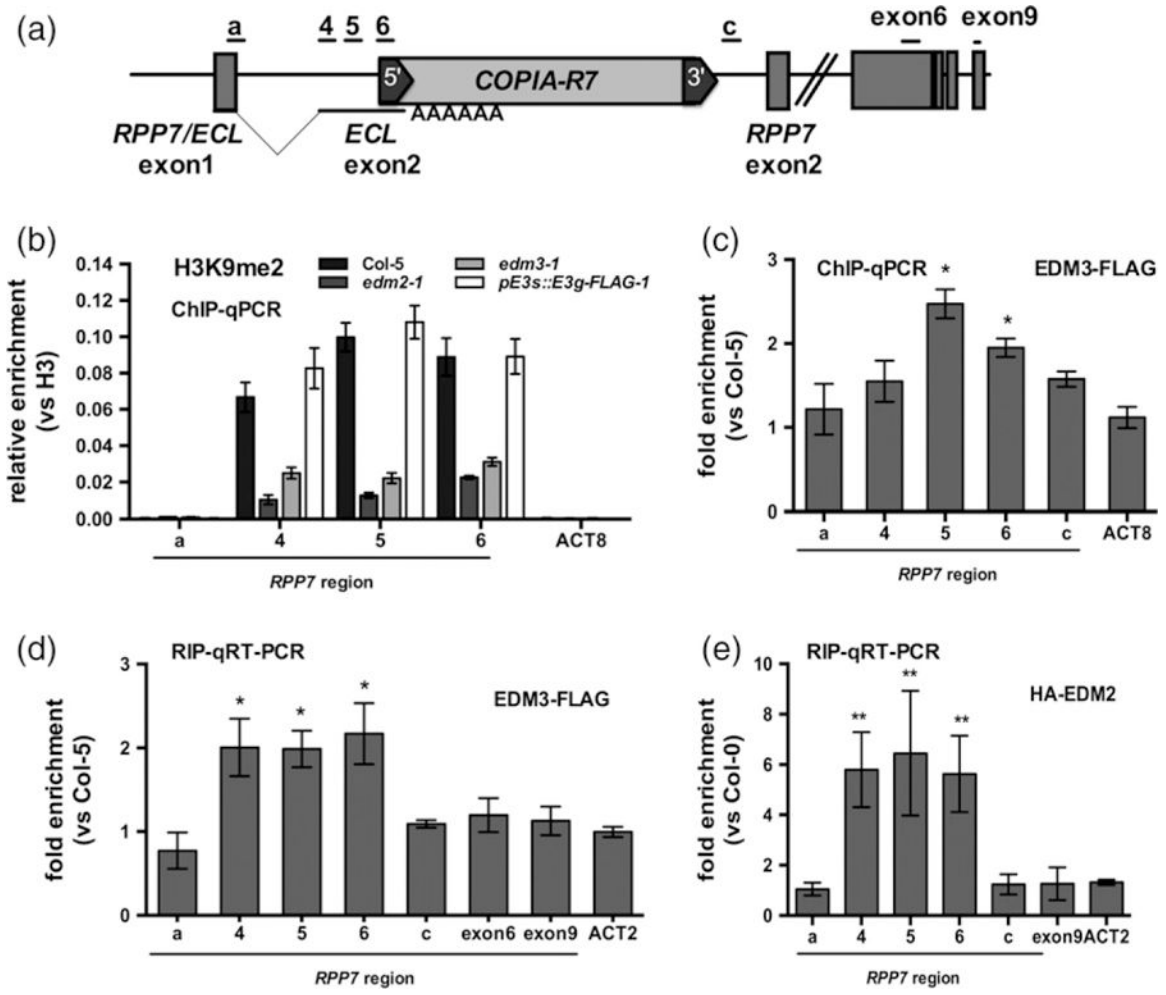

Figure 4.

RPP7 site-specific effects of EDM3.

(a) Schematic representation of the *RPP7* area studied in experiments shown below.

(b) Like EDM2, EDM3 promotes H3K9me2 at a proximal RPP7 polyadenylation site. Levels of H3K9me2 were determined by chromatin immunoprecipitation (ChIP)-quantitative polymerase chain reaction (qPCR) in Col-5, *edm2–1*, *edm3–1* and the *pE3s::E3g-FLAG-1* complementation line. H3K9me2 levels were normalized to the total histone H3 levels. *ACTIN8* (ACT8) served as a control locus. Error bars represent SEM for two biological replicates with three technical replicates each.

(c) EDM3-FLAG associates *in vivo* with RPP7 chromatin at the proximal polyadenylation site at the COPIA-R7 5'LTR. Enrichment of EDM3-FLAG at *RPP7* in the *pE3s::E3g-FLAG-1* complementation line. Levels of EDM3-FLAG were calculated relative to each area in Col-5. Error bars represent SEM for two biological replicates with three technical replicates.

(d, e) EDM3-FLAG and HA-EDM2 co-associate *in vivo* with RPP7 transcripts at the proximal polyadenylation site at the COPIA-R7 5'LTR. Levels of EDM3-FLAG or HA-EDM2 at *RPP7* were measured by RNA immunoprecipitation (RIP)-qRT-PCR relative to each area in Col-5 or Col-0, respectively. *ACTIN2* (ACT2) served as a control locus. Error

bars represent SEM for three biological replicates with three technical replicates each. * and ** indicate $P < 0.05$ and < 0.01, respectively, determined by Student's *t*-test.

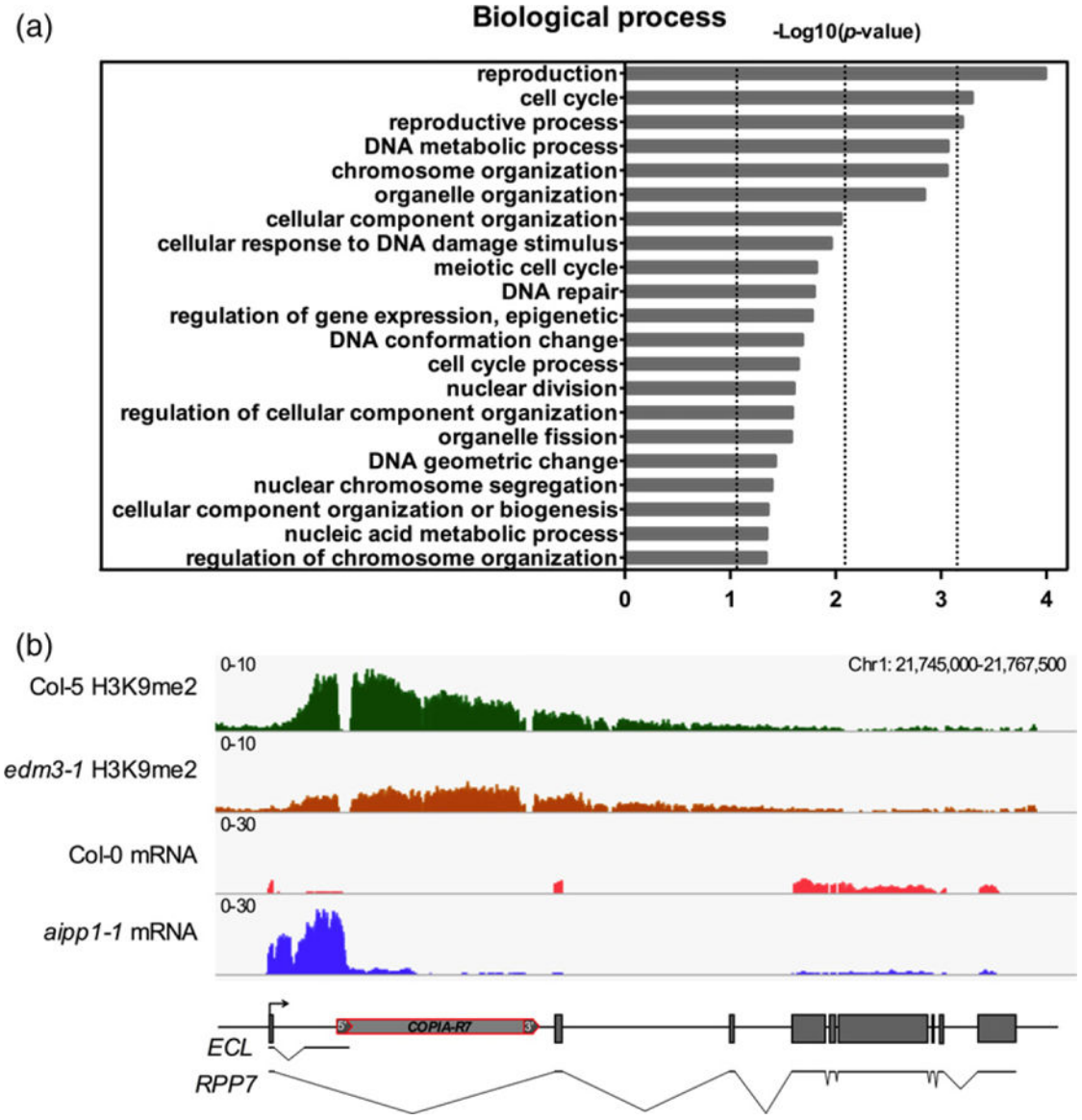

Figure 5.

EDM3 affects genome-wide levels of H3K9me2.

(a) Gene ontology (GO) term analysis with gene sets showing H3K9 hyper-dimethylation in *edm3–1* ($P < 0.05$). GO term analysis was performed using PANTHER (http://www.geneontology.org).

(b) Genome browser view of chromatin immunoprecipitation (ChIP)-seq and RNA-seq data at the *RPP7* locus. The *y*-axis represents coverage values (normalized per million mapped reads). Schematic representations of the *RPP7* locus with RNA transcript isoforms are shown at the bottom. *COPIA-R7* is labeled in the red box. ECL: 'Exon1-containing 5'LTR terminated' non-coding transcript resulting from proximal polyadenylation/transcript termination at RPP7.

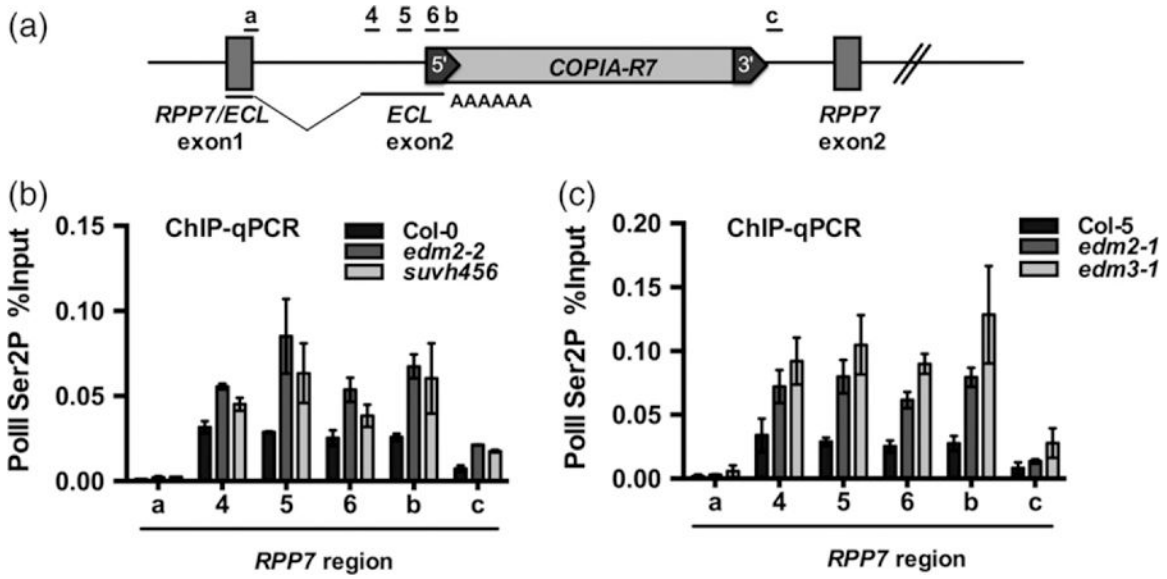

Figure 6.

EDM2 and EDM3 affect RNA polymerase II (RNAPII) progression rates at the proximal *RPP7* polyadenylation site.

(a) Schematic representation of *RPP7* area studied in experiments.

(b, c) Chromatin immunoprecipitation (ChIP)-quantitative polymerase chain reaction (qPCR) with 2-P-ser-RNAPII-specific antibodies. Occupancy of genomic DNA with 2-P-ser-RNAPII determined by ChIP-qPCR in Col-0, *edm2–2*, *suvh456* and Col-5, *edm2–1*, *edm3–1*. Levels of 2-P-ser-RNAPII were normalized to the total input. Error bars represent SEM for two biological replicates with three technical replicates.

Table 1

Asexual reproduction of three *Hyaloperonospora arabidopsidis* isolates (*Hpa*-Hiks1, *Hpa*-Cala2 and *Hpa*-Cand5) in wild-type Arabidopsis accessions, a susceptible mutant control (ws-*eds1*) and *Hpa*-Hiks1 susceptible Columbia (Col-5) mutants

	Hiks1			Cala2			Cand5		
Arabidopsis line	**No.**	**Mean**	**SEM**	**No.**	**Mean**	**SEM**	**No.**	**Mean**	**SEM**
Col-5	116	0.0	0.0	72	0.7	0.2	82	0.9	0.3
rpp7–1	144	17.9	0.4	78	0.2	0.1	138	0.8	0.2
edm2–1	124	17.7	0.4	96	0.4	0.1	84	0.1	0.0
edm3–1	138	16.1	0.5	86	0.5	0.1	80	0.2	0.1
Duc-1	78	17.2	0.5	40	0.0	0.0	64	19.8	0.1
Ksk-1	14	18.6	0.6		nt			nt	
Ws-*eds1*	76	18.1	0.5	70	19.9	0.1	70	18.7	0.6

No., number of cotyledons; Mean, mean of sporangiophores per cotyledon; SEM, standard error of the mean; nt, not tested.